diabetes®
American Diabetes Association®

Deletion of Carboxypeptidase E in β-Cells Disrupts Proinsulin Processing but Does Not Lead to Spontaneous Development of Diabetes in Mice

Yi-Chun Chen, Austin J. Taylor, James M. Fulcher, Adam C. Swensen, Xiao-Qing Dai, Mitsuhiro Komba, Kenzie L.C. Wrightson, Kenny Fok, Annette E. Patterson, Ramon I. Klein Geltink, Patrick E. MacDonald, Wei-Jun Qian, and C. Bruce Verchere

Diabetes 2023;72(9):1277–1288 | https://doi.org/10.2337/db22-0945

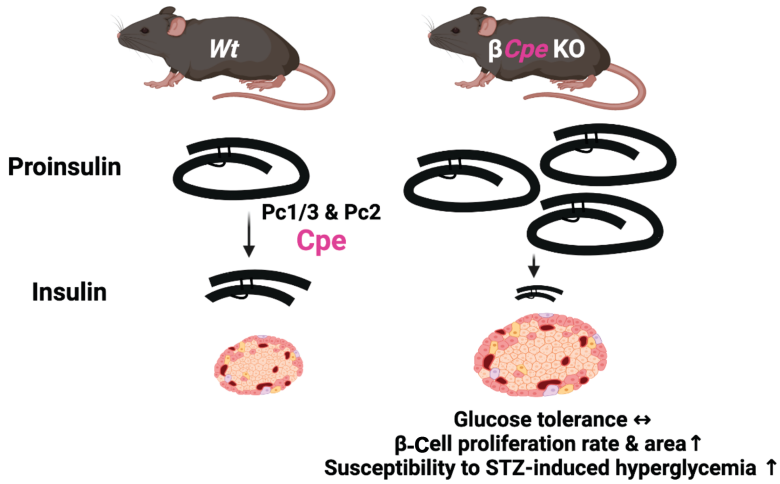

Deletion of Carboxypeptidase E in β-Cells Disrupts Proinsulin Processing but Does Not Lead to Spontaneous Development of Diabetes in Mice

Yi-Chun Chen,[1,2] Austin J. Taylor,[2,3] James M. Fulcher,[4] Adam C. Swensen,[4] Xiao-Qing Dai,[5] Mitsuhiro Komba,[1,2] Kenzie L.C. Wrightson,[2] Kenny Fok,[2] Annette E. Patterson,[2,3] Ramon I. Klein Geltink,[2,3] Patrick E. MacDonald,[5] Wei-Jun Qian,[4] and C. Bruce Verchere[1,2,3,6]

Diabetes 2023;72:1277–1288 | https://doi.org/10.2337/db22-0945

Carboxypeptidase E (CPE) facilitates the conversion of prohormones into mature hormones and is highly expressed in multiple neuroendocrine tissues. Carriers of *CPE* mutations have elevated plasma proinsulin and develop severe obesity and hyperglycemia. We aimed to determine whether loss of *Cpe* in pancreatic β-cells disrupts proinsulin processing and accelerates development of diabetes and obesity in mice. Pancreatic β-cell–specific Cpe knockout mice (β*Cpe*KO; *Cpe*$^{fl/fl}$ x *Ins1*$^{Cre/+}$) lack mature insulin granules and have elevated proinsulin in plasma; however, glucose-and KCl-stimulated insulin secretion in β*Cpe*KO islets remained intact. High-fat diet–fed β*Cpe*KO mice showed weight gain and glucose tolerance comparable with those of *Wt* littermates. Notably, β-cell area was increased in chow-fed β*Cpe*KO mice and β-cell replication was elevated in β*Cpe*KO islets. Transcriptomic analysis of β*Cpe*KO β-cells revealed elevated glycolysis and *Hif1α*-target gene expression. On high glucose challenge, β-cells from β*Cpe*KO mice showed reduced mitochondrial membrane potential, increased reactive oxygen species, reduced *MafA*, and elevated *Aldh1a3* transcript levels. Following multiple low-dose streptozotocin injections, β*Cpe*KO mice had accelerated development of hyperglycemia with reduced β-cell insulin and Glut2 expression. These findings suggest that Cpe and proper proinsulin processing are critical in maintaining β-cell function during the development of hyperglycemia.

ARTICLE HIGHLIGHTS

- Carboxypeptidase E (Cpe) is an enzyme that removes the carboxy-terminal arginine and lysine residues from peptide precursors.
- Mutations in *CPE* lead to obesity and type 2 diabetes in humans, and whole-body *Cpe* knockout or mutant mice are obese and hyperglycemic and fail to convert proinsulin to insulin.
- We show that β-cell–specific *Cpe* deletion in mice (β*Cpe*KO) does not lead to the development of obesity or hyperglycemia, even after prolonged high-fat diet treatment. However, β-cell proliferation rate and β-cell area are increased, and the development of hyperglycemia induced by multiple low-dose streptozotocin injections is accelerated in β*Cpe*KO mice.

Proinsulin is processed into mature insulin and C-peptide by prohormone convertase (PC)1/3 and PC2 and carboxypeptidase E (CPE) (1–3) prior to secretion from pancreatic β-cells. Failure of this process leads to insufficient mature insulin release and onset of hyperglycemia (4–6) and has been observed in diabetes pathogenesis (7,8).

Prohormone processing enzymes are highly expressed in neuroendocrine cells, and subjects with mutations in

[1]Department of Surgery, Faculty of Medicine, University of British Columbia, Vancouver, British Columbia, Canada
[2]BC Children's Hospital Research Institute, Vancouver, British Columbia, Canada
[3]Department of Pathology and Laboratory Medicine, Faculty of Medicine, University of British Columbia, Vancouver, British Columbia, Canada
[4]Integrative Omics, Biological Sciences Division, Pacific Northwest National Laboratory, Richland, WA
[5]Department of Pharmacology, University of Alberta, Edmonton, Alberta, Canada
[6]Centre for Molecular Medicine and Therapeutics, Faculty of Medicine, University of British Columbia, Vancouver, British Columbia, Canada

Corresponding author: C. Bruce Verchere, bverchere@bcchr.ca

Received 17 April 2023 and accepted 22 June 2023

This article contains supplementary material online at https://doi.org/10.2337/figshare.23564925.

these genes often display cognitive impairments and obesity. A *CPE* truncating mutation (c.76_98del) causes morbid obesity and severe hyperglycemia (9), a *CPE* nonconservative missense mutation (c.847C>T) reduces enzymatic activity associated with early-onset type 2 diabetes (10), and homozygous nonsense *CPE* mutations (c.405C>A) cause obesity and hypogonadotropic hypogonadism (11). Similarly, *Cpe* whole-body knockout mice develop spontaneous obesity and behavioral abnormalities (12), and *Cpe* mutant mice ($Cpe^{fat/fat}$) are obese and infertile (13).

To understand the role of *Cpe* in β-cell function and glucose homeostasis, we generated pancreatic β-cell–specific *Cpe* knockout mice. We performed biochemical and top-down proteomic analysis to evaluate hormone processing patterns in β-cells. We also analyzed β-cell transcriptomic profiles and performed live-cell imaging analysis to understand whether deficiency of *Cpe,* and the increased compensatory production of proinsulin, leads to islet dysfunction and dysglycemia. Finally, we tested whether the lack of *Cpe* in β-cells increases susceptibility to diet- or secretory stress–induced hyperglycemia in mice. Our model provides a useful tool to understand the role of reduced prohormone processing efficiency and increased (pro)insulin translation in β-cells during diabetes development and sheds light on whether impaired prohormone processing in β-cells is a cause of diabetes and obesity in subjects with *CPE* mutations.

RESEARCH DESIGN AND METHODS

Human Pancreas Tissue

Paraffin-embedded pancreatic tissue sections were obtained from the Network for Pancreatic Organ donors with Diabetes (nPOD) and Alberta Diabetes Institute IsletCore (Supplementary Table 1).

Mouse Studies

β-Cell–specific *Cpe* knockout (β*Cpe*KO) and inducible β-cell–specific *Cpe* knockout (iβ*Cpe*KO) mice were generated through crossing the offspring of C57BL/6N-$Cpe^{tm1a(EUCOMM)Hmgu}$/Ieg mice and Tg(CAG-flpo)1Afst mice with B6(Cg)-$Ins1^{tm1.1(cre)Thor}$/J or Tg(Pdx1-cre/Esr1) mice. In addition, *Gt(ROSA)26Sor*$^{tm4(ACTB-tdTomato,-EGFP)Luo}$ reporter mice were bred with β*Cpe*KO mice for β-cell sorting and RNA sequencing. The control mice used for biochemical, imaging, and metabolic experiments are as follows: $Ins1^{Cre/+}$;$Cpe^{fl/+}$ (β*Cpe*Het) as well as $Ins1^{+/+}$;$Cpe^{fl/fl}$ or $Ins1^{+/+}$;$Cpe^{fl/+}$ (*Wt*). For diet studies, 8-week-old mice received either a low-fat diet (LFD) (10% fat), or a high-fat diet (HFD) (45% fat; Research Diets). For secretory stress studies, 10-week-old male mice received saline or streptozotocin (STZ): multiple injections of low-dose STZ (MLD-STZ) (35 mg/kg body wt i.p. daily for 5 days; Sigma-Aldrich). Metabolic assays (such as intraperitoneal glucose tolerance test (IPGTT), insulin tolerance test (ITT), and body mass composition analysis) were performed in a blinded fashion and have previously been described (14). For in vivo β-cell proliferation studies, after tamoxifen-induced *Cpe* deletion, a 60% fat diet (Research Diets) was given for 48 h (15) in combination with 5-ethynyl-2'-deoxyuridine (40 mg/kg body wt i.p. injection twice daily, EdU; Toronto Research Chemicals) (16). All studies were approved by the Animal Care and Use Committee at the University of British Columbia.

Islet Studies

Mouse islets were isolated and cultured as previously described (14). For electron micrograph studies, freshly isolated islets were fixed in 2% glutaraldehyde (pH 7.4) at room temperature, shipped, processed, and imaged by the Electron Microscopy Facility at McMaster University Health Science Centre. PC1/3 and PC2 enzyme activity assays were performed as previously described (17) with a SpectraMax M3 plate reader (Molecular Devices). For respirometry studies, mouse islets were dispersed and analyzed by Seahorse XFe96 Analyzer (Agilent Technologies). For analysis of insulin secretion dynamics, islets were incubated in a perifusion system (Biorep Technologies) with 1.67 mmol/L glucose, 1.67 mmol/L glucose, and 16.7 mmol/L glucose plus 30 mmol/L KCl Krebs-Ringer buffer sequentially. Insulin concentrations in perifusates were analyzed with rodent insulin (ALPCO) and proinsulin (Mercodia) ELISAs. For measurement of glucose uptake, islets were precultured in glucose-free media, dispersed with Accutase (Innovative Cell Technologies), and treated with 2-NBDG (2-deoxy-2-[(7-nitro-2,1,3-benzoxadiazol-4-yl)amino]-D-glucose; Invitrogen) for 5 min, prior to flow cytometry analysis.

For exocytosis studies, dispersed islet β-cells were patch clamped in whole-cell voltage-clamp configuration with use of a HEKA EPC 10 amplifier and PATCHMASTER software (HEKA Electronik, Lambrecht, Germany) as previously described (18). Exocytosis was monitored as increases in cell capacitance, elicited by either a series of 500-ms membrane depolarizations from −70 to 0 mV or increase in the duration of membrane depolarizations. For FACS-sorted β-cell bulk-RNA sequencing experiments, freshly isolated islets were dispersed and GFP^+ live cells were collected with BD FACSAria Cell Sorter for RNA isolation via an RNeasy Plus Micro Kit (QIAGEN). After quality control analysis with an Agilent 2100 Bioanalyzer, an RNA library was prepared with use of the NeoPrep Library Prep system with TruSeq Stranded mRNA kit (Illumina); RNA sequencing was performed with Illumina NextSeq 500; reads were aligned with TopHat to the reference genome of UCSC Genome Browser mm10, assembled by Cufflinks; and a list of differentially expressed genes was generated via DESeq2. Gene set enrichment analysis, network visualization, and volcano plot were generated via Gene Set Enrichment Analysis (GSEA v4.2.3), Cytoscape (v3.9.1), and EnhancedVolcano (v1.14.0) in RStudio (v1.4.1717).

Top-down Proteomic Analysis

Islet pellets were homogenized in 8 mol/L urea lysis buffer, reduced, alkylated, quenched, and clarified with

tris(2-carboxyethyl)phosphine, iodoacetamide, and dithiothreitol, before 3 kDa molecular weight cutoff filtration. Samples were analyzed with a Waters nanoACQUITY UPLC system with mobile phases consisting of 0.2% formic acid in H2O and 0.2% formic acid in acetonitrile. For tandem mass spectrometry analysis of proteins, the nanoACQUITY UPLC system was coupled to a Thermo Scientific Orbitrap Fusion Lumos mass spectrometer equipped with the FAIMS Pro interface (19). Proteoform identification was performed with TopPIC (v1.4). Downstream data analysis and quantification were performed with use of MSstats (v4.0.1) and TopPICR (v0.0.3) R packages.

Immunoblot Studies

Mouse islets were lysed in an NP-40–based buffer and analyzed through reducing or nonreducing Tricine–urea–SDS-PAGE (20), and blotted with use of antibodies listed in Supplementary Table 2, on a LI-COR Biosciences Odyssey Imaging System. For analysis of insulin biosynthesis, islets were preincubated in methionine-free RPMI medium for 90 min and then treated with L-azidohomoalaine (Invitrogen) and 5 or 25 mmol/L glucose Krebs-Ringer buffer for 90 min. Islets were lysed, click labeled with biotin-alkyne (Invitrogen), and immunoprecipitated and the eluted proteins were analyzed on a Tricine–urea–SDS-PAGE system.

Immunostaining and Image Analysis

Dispersed mouse islet cells were seeded on chamber slides (ibidi or Thermo Fisher Scientific) overnight and cultured in 5 or 25 mmol/L glucose RPMI media for the indicated times. For cell proliferation experiments, EdU was added during the last 24 h of treatment, followed by click labeling and staining (Invitrogen). TUNEL staining was performed according to the manufacturer's manual (Roche). For live-cell imaging experiments, cells were labeled with CellROX, MitoSOX, tetramethylrhodamine methyl ester (TMRM) (Thermo Fisher Scientific), and MitoTracker Green (MTG) (New England Biolabs) and imaged with use of an SP5II laser scanning confocal microscope (Leica Microsystems). Cpd and proinsulin costained β-cells were imaged on an SP8 X STED (STimulated Emission Depletion) white light laser confocal imaging system. β-Cell area was analyzed with immunohistochemistry staining against insulin with a BX61 microscope (Olympus). All antibodies used are listed in Supplementary Table 2. Image analyses were performed with ImageJ (21), QuPath, ilastik, and CellProfiler pipelines.

Quantitative RT-PCR Experiments

Islet mRNA and DNA were isolated with PureLink RNA Micro (Invitrogen) and QIAamp DNA Micro (QIAGEN) kits, and cDNA was synthesized with a SuperScript VILO kit (Invitrogen). mRNA and DNA levels were analyzed with SYBR Green–based quantitative real-time PCR (ViiA 7 Real-Time PCR System; Applied Biosystems). Primer sequences are listed in Supplementary Table 2.

Statistical Analysis

Statistical analyses were performed through GraphPad Prism 9 or R. After normality tests, data sets with normal distribution or with small sample numbers were analyzed using Student *t* test or ANOVA followed by post hoc analysis. Data with nonnormal distribution were analyzed with the Wilcoxon rank sum test. Statistical significance is indicated in the figures as follows: $*P < 0.05$. All data are presented as mean ± SEM.

Data and Resource Availability

Data and reagents generated in the current study are available from the corresponding author on reasonable request.

RESULTS

Loss of Mature Insulin Granules and Elevated Plasma Proinsulin in β*Cpe*KO Mice

CPE is highly expressed in human and mouse islet endocrine cells (Fig. 1*A* and *B*). To study the roles of Cpe in β-cells, we generated β*Cpe*KO mice by crossing *Ins1*$^{Cre/+}$ and *Cpe*$^{fl/fl}$ mice (Fig. 1*C–E*). The deletion of *Cpe* in β-cells leads to near-total loss of mature insulin granules (Fig. 1*F*) and significantly elevated fasting plasma proinsulin-like immunoreactivity (Fig. 1*G* and *H*). As most immunoassays likely cross-react with target peptide with various C- and N-terminal extensions, we decided to analyze the propeptide repertoire with biochemical and proteomic approaches.

Permissive Peptide Processing in β*Cpe*KO Islets

Proinsulin is first processed by PC1/3 to form split-32,33 proinsulin with overhanging basic residues. Cpe then removes these basic residues to yield the des-31,32 proinsulin intermediate, which is cleaved by PC2 (or PC1/3) to produce mature insulin following trimming of the remaining basic residues by Cpe (1–3). To study the impact of β-cell Cpe deficiency on proinsulin processing, we analyzed proinsulin forms using a nonreducing SDS-PAGE system. We found that higher-molecular-weight proinsulin forms were increased in β*Cpe*KO islets. The lower bands are likely the combination of mature insulin and insulin with basic residue extensions, as their molecular weights are similar and may not be separated by electrophoresis. (Fig. 2*A*). Similar to proinsulin, islet amyloid polypeptide (IAPP) is also synthesized as a larger precursor, proIAPP, and is processed by PC1/3, PC2, Cpe, and Pam to form amidated IAPP (14,22–24). Nonamidated IAPP and intermediate proIAPP (proIAPP$_{1–48}$) forms are increased in β*Cpe*KO islets, although amidated IAPP levels appear comparable between *Wt* and β*Cpe*KO islets (Fig. 2*B*). Proteomic assessment confirmed that intact proinsulin levels are increased in β*Cpe*KO islets, while levels of the mature insulin are reduced (Fig. 2*C* and *D*). Full-length proIAPP levels are also increased, while levels of amidated mature IAPP level are not reduced, in β*Cpe*KO islets (Fig. 2*E* and *F*).

To determine whether *Cpe* deletion creates feedback inhibition of peptide hormone maturation, we analyzed

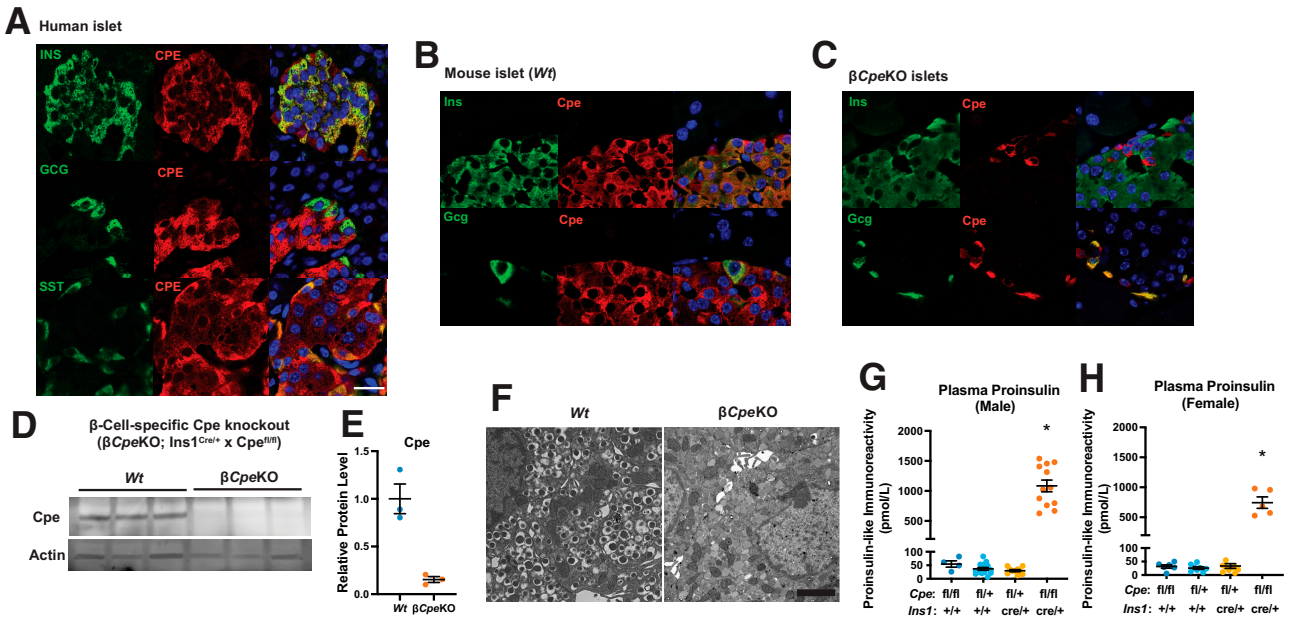

Figure 1—Elevated proinsulin levels in β*Cpe*KO mice. *A–C*: Expression of CPE in human and mouse pancreatic islet cells was analyzed via immunostaining with antibodies against CPE, insulin (INS), glucagon (GCG), and somatostatin (SST). *D* and *E*: Cpe expression in β*Cpe*KO mice was analyzed through immunoblotting (n = 3 and 3) with an antibody against Cpe. *F*: Representative electron micrographs of β-cells from *Wt* and β*Cpe*KO mice. Scale bar = 2 μm (n = 3 and 3). *G* and *H*: 4-h fasting plasma proinsulin levels in β*Cpe*KO and littermate male and female mice ($n > 4$ per genotype group per sex).

prohormone processing enzyme transcript and protein levels. Expression of insulin, IAPP, and processing enzyme transcripts are comparable between β*Cpe*KO and *Wt* islets (Fig. 2*G*). ProPC1/3 protein (87 kDa) levels are elevated, as are PC2 and proSAAS (Fig. 2*H* and *I*); however, total islet PC1/3-specific activity is not changed (Fig. 2*J*). PC2-specific activity is reduced in β*Cpe*KO mice (Fig. 2*K*), which may occur through increased 7B2-mediated inhibition of PC2 activity (25). We also found that Cpe is not the only carboxypeptidase capable of processing peptide hormones in β-cells. Despite near-complete recombination and deletion of *Cpe* (Fig. 1*C–E*), mature insulin remains detectable, and mature IAPP is expressed at levels similar to those of *Wt* islets (Fig. 2*B*). Carboxypeptidase D (CPD) has been detected in the Golgi network of rodent β-cells (26) and may not be removed from immature insulin granules in conditions such as cargo protein CCDC186 deficiency (27). CPD is expressed in human islet β-cells (Fig. 2*L*). Increased presence of Cpd in proinsulin-containing organelles such as the Golgi network or immature insulin granules may aid the processing of prohormones in the absence of Cpe, as the colocalization of Cpd and proinsulin is significantly higher in Cpe-deficient β-cells (Fig. 2*M* and *N*).

β*Cpe*KO Mice Do Not Develop Diet-Induced Obesity and Diabetes

Unlike *Cpe* whole-body knockout mice or *Cpe* mutant mice (12,13), 8 week-old β*Cpe*KO mice do not develop early-onset obesity and diabetes (males [Fig. 3*A–C*] and females [Fig. 3*D–F*]). Islets from β*Cpe*KO mice displayed insulin secretion dynamics comparable with those of *Wt* islets (Fig. 3*G*), speaking against a role for Cpe as a granule-sorting receptor in β-cells. Interestingly, proinsulin was released upon high glucose and KCl stimulation (Fig. 3*H*), suggesting that the proinsulin-containing granules are likely equipped with appropriate granule contents that allow for efficient granule release. Rates of exocytosis were also comparable between *Wt* and *Cpe*-deficient β-cells (Fig. 3*I*), although exocytosis events proximal to the plasma membrane, measured by a time-train depolarization experiment, were slightly reduced in β-cells from β*Cpe*KO mice (Fig. 3*J*).

To promote the development of obesity and insulin resistance, we placed 8-week-old β*Cpe*KO mice on a control LFD (10% fat) or HFD (45% fat) for a duration of 6 months. In the LFD-treated group, weight gain of β*Cpe*KO mice was similar to that of their *Wt* littermates (males [Fig. 4*A*] and females [Fig. 4*F*]), suggesting that the lack of *Cpe* in β-cells does not lead to spontaneous development of obesity. At 20 weeks post-LFD, male β*Cpe*KO mice displayed modestly increased fasting blood glucose levels (Fig. 4*B*); however, their glucose tolerance, insulin tolerance, and percent fat mass, measured at 16 weeks and 20 weeks post-LFD, remained comparable with those of *Wt* littermates (Fig. 4*C–E*). Female β*Cpe*KO mice have slightly elevated fasting blood glucose levels at 4 and 22 weeks post-LFD, yet displayed glucose tolerance, insulin tolerance, and body fat mass similar to those of littermates (Fig. 4*G–J*). Inappropriate proinsulin processing associated with β-cell *Cpe* deficiency does not contribute to accelerated development of HFD-induced obesity (males [Fig. 4*K*] and females [Fig. 4*P*]). Male and female β*Cpe*KO

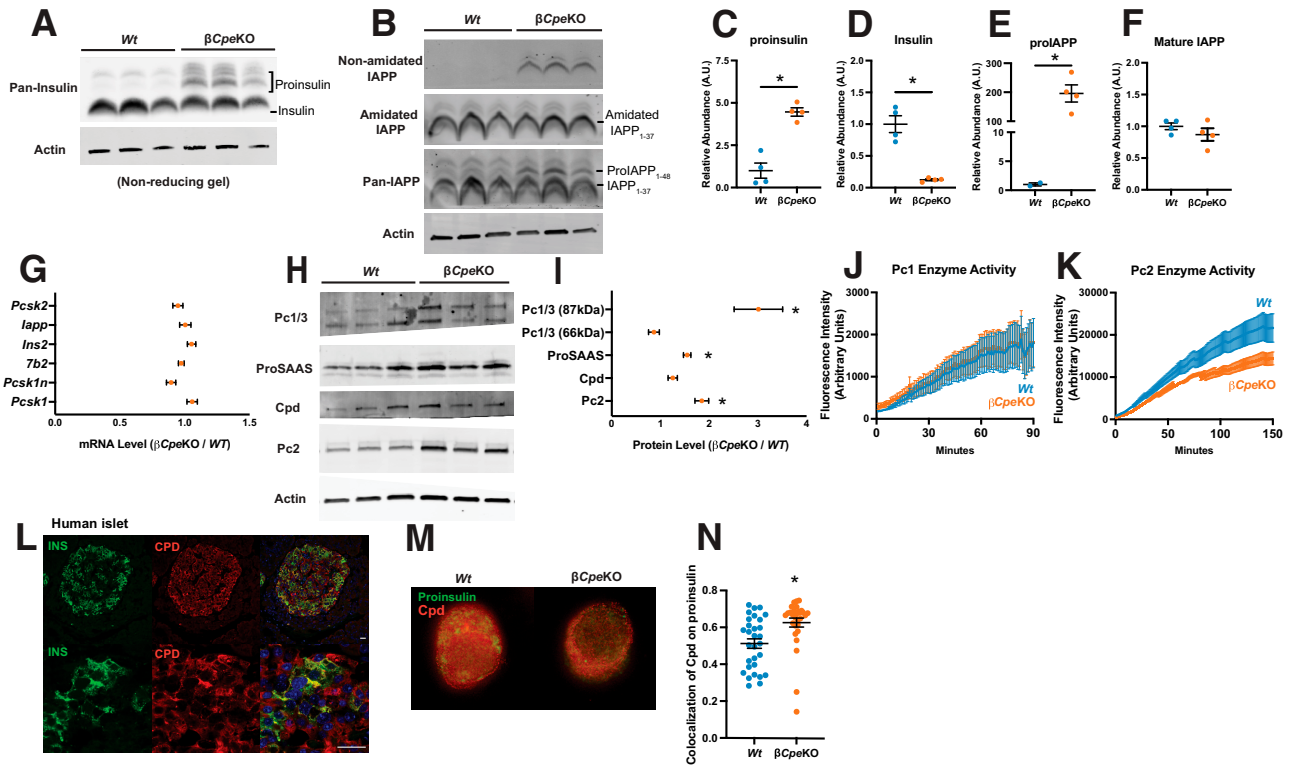

Figure 2—Impaired prohormone processing in β*Cpe*KO islets. *A*: We analyzed islet (pro)insulin levels by nonreducing SDS-PAGE and immunoblotting using an antibody against insulin. *B*: Islet (pro)IAPP levels were analyzed through immunoblotting with use of antibodies against nonamidated IAPP, amidated IAPP, and IAPP. *C–F*: Quantification of full-length proinsulin, mature insulin B-chain fragment, full-length proIAPP, and amidated mature IAPP with a top-down proteomics assay by mass spectrometry (n = 4 and 4). *G*: mRNA levels of *Pcsk2*, *Iapp*, *Ins2*, *7b2*, *Pcsk1n*, and *Pcsk1* in β*Cpe*KO were analyzed with quantitative RT-PCR and are presented as folds over *Wt* (n = 6 and 6). *H* and *I*: Protein levels of proPC1/3 (87kDa), PC1/3 (66 kDa), full-length proSAAS, Cpd, and PC2 were analyzed through immunoblotting with use of antibodies against PC1/3, proSAAS, Cpd, and PC2 (n = 3 and 3). *J* and *K*: We measured islet PC1/3 and PC2 enzyme activities by cleavage of synthetic fluorogenic enzyme substrates (n = 3 and 3). *L*: Expression of CPD in human islets β-cells was analyzed with immunostaining with use of antibodies against Cpd and insulin. Scale bar = 25 μm. *M* and *N*: Immunofluorescence staining of proinsulin and Cpd in *Wt* and β*Cpe*KO β-cells was captured by STED microscope (10 consecutive z stack images per cell were taken from mice with different genotypes, three cells were analyzed per genotype), and colocalization of proinsulin and Cpd was analyzed with the Manders method. A.U., arbitrary units.

mice showed fasting blood glucose levels, glucose tolerance, insulin tolerance, and percent fat mass similar to those of their littermates (Fig. 4*L–O* and *Q–T*).

Increased β-Cell Proliferation in *Cpe*-Deficient Mice

Despite comparable glucose tolerance, β-cell area in LFD-treated β*Cpe*KO male and female mice was elevated (Fig. 5*A* and *B*). Although HFD promoted compensatory β-cell expansion in *Wt* mice, β*Cpe*KO mice did not have an increase in β-cell area (Fig. 5*C* and *D*). To study the cause of increased β-cell area in β*Cpe*KO mice on LFD, we first examined the β-cell proliferation rate by analyzing the frequency of Ki67$^+$ β-cells. However, the number of proliferating β-cells in mice fed LFD for 6 months was too low to allow for appropriate comparison between β*Cpe*KO and *Wt* mice (data not shown). We therefore isolated islets from 10-week-old mice, cultured them in 5 or 20 mmol/L glucose media for 72 h, and analyzed EdU incorporation in insulin$^+$ β-cells. β-Cell proliferation was significantly elevated in islets from β*Cpe*KO mice (Fig. 5*E*). We also generated iβ*Cpe*KO mice by crossing *Pdx1-Cre*^{ER} mice with *Cpe*$^{flox/flox}$ mice (Fig. 5*F*). Shortly after oral tamoxifen administration, male, but not female, iβ*Cpe*KO mice become mildly glucose intolerant (Fig. 5*G* and *H*). To induce β-cell proliferation, we treated iβ*Cpe*KO and their *Wt* littermates with a 60% fat diet for 2 days and analyzed EdU incorporation in the mouse pancreas. We found that the β-cell proliferation rate was significantly elevated in iβ*Cpe*KO female mice (Fig. 5*I* [males] and Fig. 5*J* [females]).

Altered Glycolytic Gene Expression and Increased (Pro)insulin Biosynthesis in *Cpe*-Deficient β-Cells

To identify the underlying molecular mechanisms contributing to increased β-cell proliferation in β*Cpe*KO mice, we performed transcriptomic analysis in sorted β-cells from *Wt* and β*Cpe*KO mice (Fig. 6*A*). As expected, *Cpe* was drastically reduced in β-cells from β*Cpe*KO mice. Expression of many Hif1α-regulated genes (including *Ldha*, *Hmox1*, *P4ha1*, *Pgk1*, *Mif*, *Ak4*, *Bnip3*, *Pfkp*, *P4ha2*, *Slc2a1*, and *Pfkfb3*) was increased. Gene ontology analysis showed that expression of

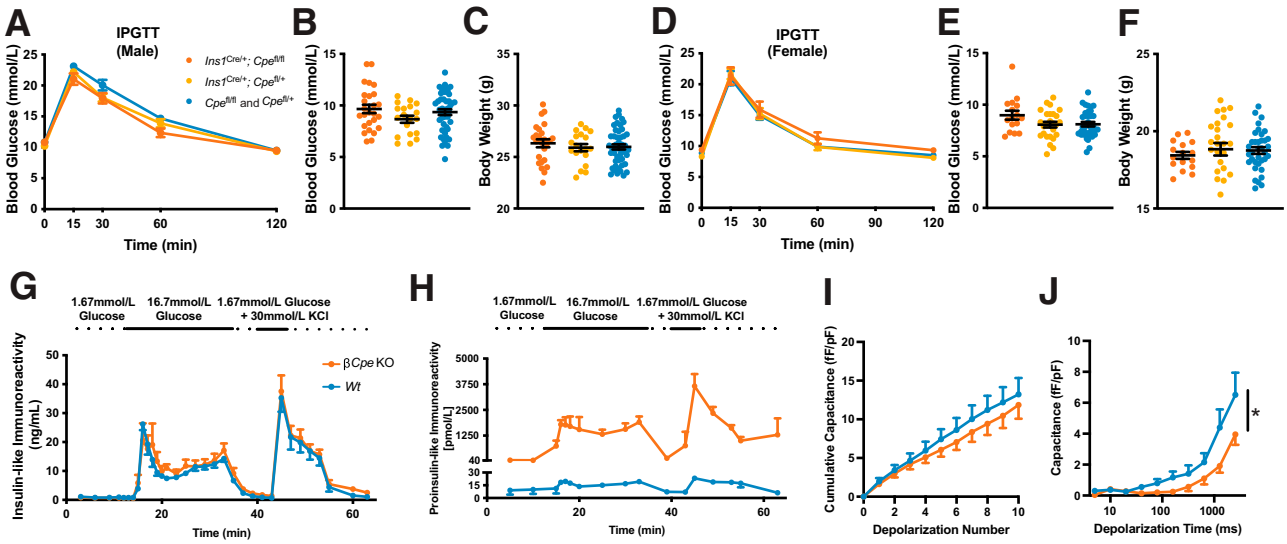

Figure 3—Glucose tolerance and insulin secretion of β*Cpe*KO mice. *A*: IPGTT was performed on 8-week-old chow-fed β*Cpe*KO and littermate males ($n \geq 5$ per genotype). *B* and *C*: 4-h fasting blood glucose levels and body weight of 8-week-old chow-fed β*Cpe*KO and littermate males ($n \geq 5$ per genotype). *D*: IPGTT was performed on 8-week-old chow-fed β*Cpe*KO and littermate females ($n \geq 6$ per genotype). *E* and *F*: 4-h fasting blood glucose and body weight of 8-week-old chow-fed β*Cpe*KO and littermate females ($n \geq 6$ per genotype). *G* and *H*: Insulin-like immunoreactivity and proinsulin-like immunoreactivity during perifusion of 1.67 mmol/L glucose, 16.7 mmol/L glucose, and 1.67 mmol/L glucose plus 30 mmol/L KCl ($n = 5$ and 5). *I* and *J*: Exocytosis, and exocytosis during a train of depolarization pulses with increased duration, of β-cells from islets of β*Cpe*KO and *Wt* mice (>10 cells per mouse, three mice per genotype).

genes related to glycolysis and hypoxia are enriched, while hallmarks of pancreatic β-cells are reduced, in *Cpe*-deficient mouse β-cells (Fig. 6*B*). We found that the rate of glucose uptake into islet cells is comparable in β*Cpe*KO and *Wt* mice (Fig. 6*C*), and glycolytic flux analysis showed that β*Cpe*KO islet cells have an oxygen consumption rate similar to that of *Wt* islet cells (Fig. 6*D*). Interestingly, despite elevated (pro)insulin production (Fig. 6*E*) and increased accumulation of proinsulin oligomers (28) (Fig. 6*F*), (pro)insulin protein stability was not significantly reduced in islets from β*Cpe*KO mice (Supplementary Fig. 1), and canonical unfolded protein response elements were not elevated in freshly isolated β*Cpe*KO islets (Supplementary Fig. 2*A*–*E*).

Dysregulated Mitochondrial Dynamics and Loss of β-Cell Identity in Glucose-Challenged β*Cpe*KO Islets

Because (pro)insulin production is elevated in β*Cpe*KO islets, we asked whether the morphology or function of the fuel-providing mitochondria is altered in *Cpe*-deficient β-cells. Electron micrograph analysis of mitochondrial images showed that β*Cpe*KO β-cells have similar area, yet reduced size (Fig. 7*A*–*C*). Additional confocal image analysis showed mitochondrial number, area, perimeter, and branch number were all reduced in β*Cpe*KO β-cells (Fig. 7*D*–*H*), while mtDNA content was not reduced (Fig. 7*I*). This suggests that mitochondria in *Cpe*-deficient β-cells work to accommodate an increased demand for (pro)insulin synthesis. Nevertheless, after prolonged glucose treatment, β-cells from β*Cpe*KO mice had reduced mitochondrial membrane potential upon high glucose stimulation (Fig. 7*J*) and displayed elevated levels of mitochondrial and cellular reactive oxygen species (ROS) (Fig. 7*K* and *L*). β-Cells from β*Cpe*KO mice have no increase in mitochondria biogenesis upon high glucose culture, as *Pgc1a* transcript levels are not significantly elevated (Fig. 7*M*). Islets from β*Cpe*KO mice failed to display elevated *MafA* transcript level upon high glucose treatment (Fig. 7*N*). Rather, *Aldh1a3* transcript levels were significantly elevated, suggesting loss of β-cell identity in β*Cpe*KO islets (Fig. 7*O*). Glucose metabolism was likely altered, as transcript levels of *Pfkp* were significantly increased in β*Cpe*KO islets (Fig. 7*P*). Of note, treatment of islets with high glucose led to increased expression of endoplasmic reticulum (ER) stress markers such as spliced *Xbp1* (*Xbp1s*), but β*Cpe*KO islets showed no increase in *Xbp1s* (Fig. 7*Q*), inferring that elevated proinsulin biosynthesis does not contribute to increased ER stress in *Cpe*-deficient β-cells.

β*Cpe*KO Mice Have Accelerated Development of STZ-Induced Hyperglycemia

We administered β*Cpe*KO and littermate mice with MLD-STZ to induce cell dysfunction in a small portion of β-cells and to create secretory stress in the remaining cells (Fig. 8*A*). β*Cpe*KO mice showed higher blood glucose levels at 10 days after the last STZ treatment, compared with *Cpe* heterozygous (β*Cpe*Het) or *Wt* mice (Fig. 8*B*–*D*). β*Cpe*KO mice did not display increased STZ-induced β-cell death: β-cell area (analyzed at 10 days post-STZ) and number of TUNEL$^+$ β-cells (analyzed at 3 days post-STZ) were similar in β*Cpe*KO and *Wt* mice (Fig. 8*E* and *F*). Building on our finding of increased β-cell area in β*Cpe*KO mice (Fig. 5*A*), we found that buffer-treated β*Cpe*KO mice had a higher percentage of β-cells in their islets (Fig. 8*G*). Although

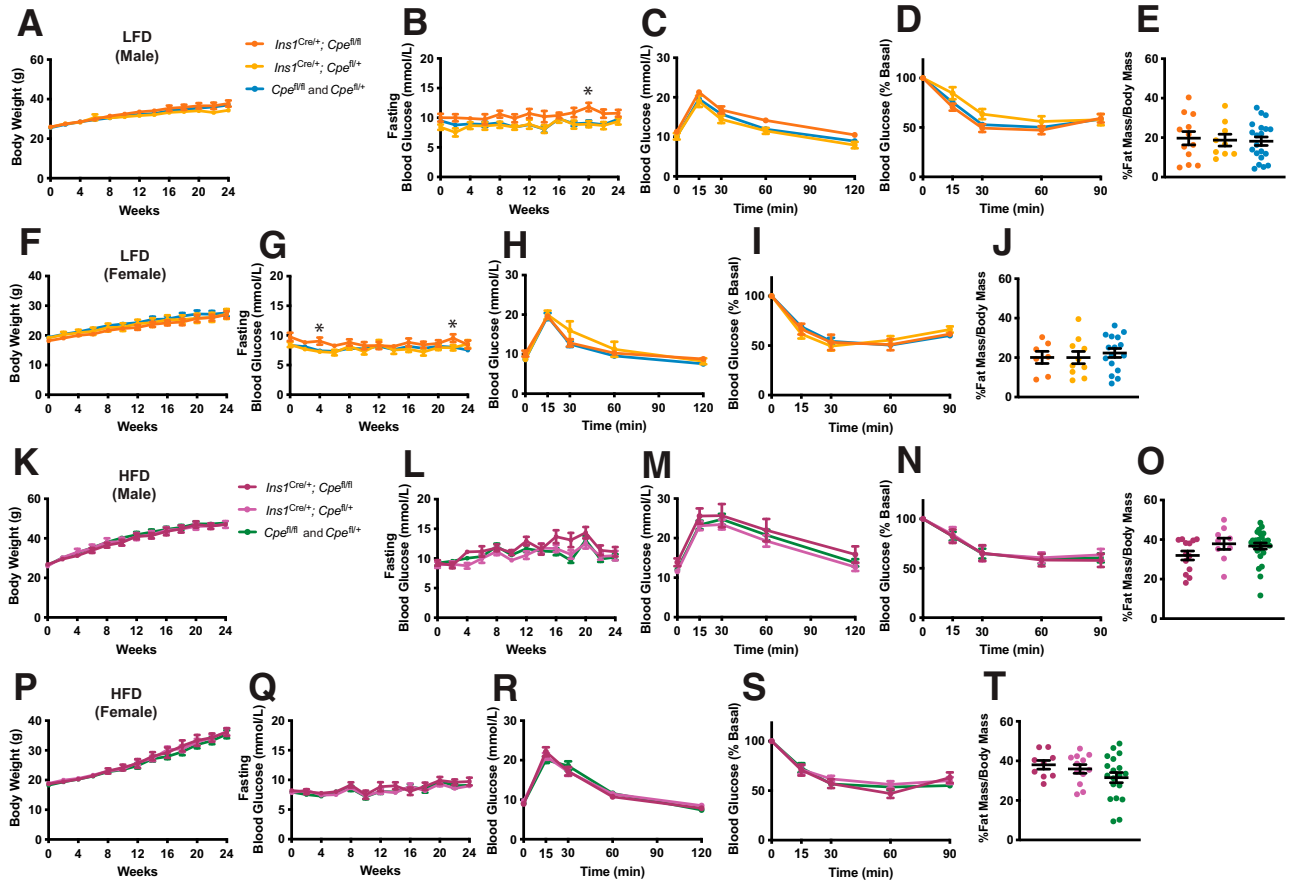

Figure 4—Comparable glucose tolerance and weight gain in HFD-fed β*Cpe*KO and littermate mice. Body weight and 4-h fasting blood glucose were monitored every 2 weeks for 24 weeks for LFD-fed β*Cpe*KO and their littermate male (*A* and *B*) and female (*F* and *G*) mice. IPGTT was performed after 16 weeks of LFD treatment on male (*C*) and female (*H*) mice. ITT and body mass composition analysis were performed after 20 weeks of LFD treatment on male (*D* and *E*) and female (*I* and *J*) mice ($n \geq 8$ per group). Body weight and 4-h fasting blood glucose were monitored every 2 weeks for 24 weeks, on HFD-fed β*Cpe*KO and their littermate male (*K* and *L*) and female (*P* and *Q*) mice. IPGTT was performed after 16 weeks of HFD treatment on male (*M*) and female (*R*) mice. ITT and body mass composition analysis were performed after 20 weeks of HFD treatment on male (*N* and *O*) and female (*S* and *T*) mice ($n \geq 8$ per group).

MLD-STZ led to a modest increase in the percentage of β-cells in *Wt* islets, it reduced the percentage of β-cells in β*Cpe*KO islets (Fig. 8*G*). In agreement with previous reports, we showed that the portion of $Glut2^+$ β-cells was reduced after MLD-STZ (Fig. 8*H*); however, the number of $Glut2^+$ β-cells remained comparable in *Wt* and β*Cpe*KO mice. We also found an increased percentage of $Aldh1a3^+$ β-cells and increased ER stress markers in the islet cells upon MLD-STZ treatment (Fig. 8*I* and Supplementary Fig. 2*F*). However, the deficiency of *Cpe* in β-cells did not cause further elevation of ER stress, as immunofluorescence intensity of phosphorylated eIF2α, Atf4, and Bip was comparable between MLD-STZ *Wt* and β*Cpe*KO mice (Supplementary Fig. 2). As the insulin antibody used for immunostaining recognizes both proinsulin and mature insulin, the increased mean fluorescence intensity observed in β-cells from buffer-treated β*Cpe*KO versus *Wt* mice likely reflects the significantly elevated proinsulin protein expression in β*Cpe*KO islets (Fig. 8*J*). Upon STZ treatment, insulin and Glut2 expression levels were significantly reduced in β*Cpe*KO, but not *Wt*, mice (Fig. 8*J* and *K*), suggesting that β-cells in β*Cpe*KO are more susceptible to secretory stress–induced degranulation and dysfunction. β-Cell maturity remained comparable, as islet Aldh1a3 expression levels were not further increased in STZ-treated β*Cpe*KO mice (Fig. 8*L*).

DISCUSSION

Cpe mutations in mice and humans lead to obesity and hyperglycemia; however, the underlying cellular and physiological mechanisms remain unknown. We hypothesized that lack of *Cpe* in pancreatic β-cells is the main contributor to such clinical phenotypes because *1*) Cpe is required for proper proinsulin processing (3), *2*) reduced expression of Cpe is associated with β-cell dysfunction in multiple experimental models of diabetes (29–31), and *3*) Cpe may play a protective role in preventing β-cell death (32). To address this hypothesis, we generated β-cell–specific *Cpe* knockout mice. Our data indicate that while Cpe is

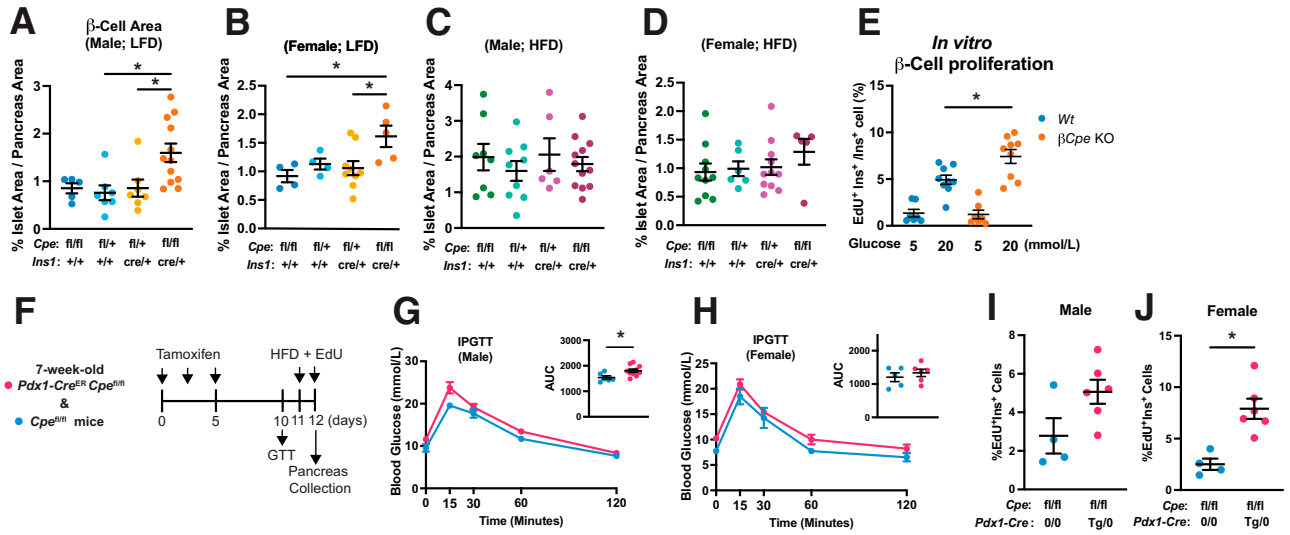

Figure 5—β*Cpe*KO mice have increased β-cell area and β-cell replication. *A–D*: β-Cell area was analyzed with insulin immunostaining of pancreatic sections from male or female β*Cpe*KO and littermate mice after 24 weeks of LFD or HFD ($n \geq 4$ per group). *E*: We analyzed β-cell replication rate by calculating EdU^+ and $insulin^+$ cells in dispersed β*Cpe*KO and *Wt* islets treated with 5 mmol/L glucose or 20 mmol/L glucose for 72 h ($n \geq 7$ per group). *F*: Timeline of in vivo β-cell replication experiment. *G* and *H*: IPGTT was performed in inducible β-cell–specific Cpe knockout mice 5 days after last tamoxifen gavage ($n \geq 5$ per group). *I* and *J*: β-Cell replication rate was analyzed by calculating EdU^+ and $insulin^+$ cells in pancreatic sections from β*Cpe*KO and *Wt* male or female mice treated with 60% HFD for 48 h ($n \geq 4$ per group). AUC, area under the curve; GTT, glucose tolerance test; wk, week.

important in normal proinsulin processing, Cpe deficiency alone does not contribute to obesity or cause marked dysglycemia.

Islets from β*Cpe*KO mice contain markedly more proinsulin peptides, yet have detectable mature insulin peptide, suggesting that another carboxypeptidase, likely Cpd, is

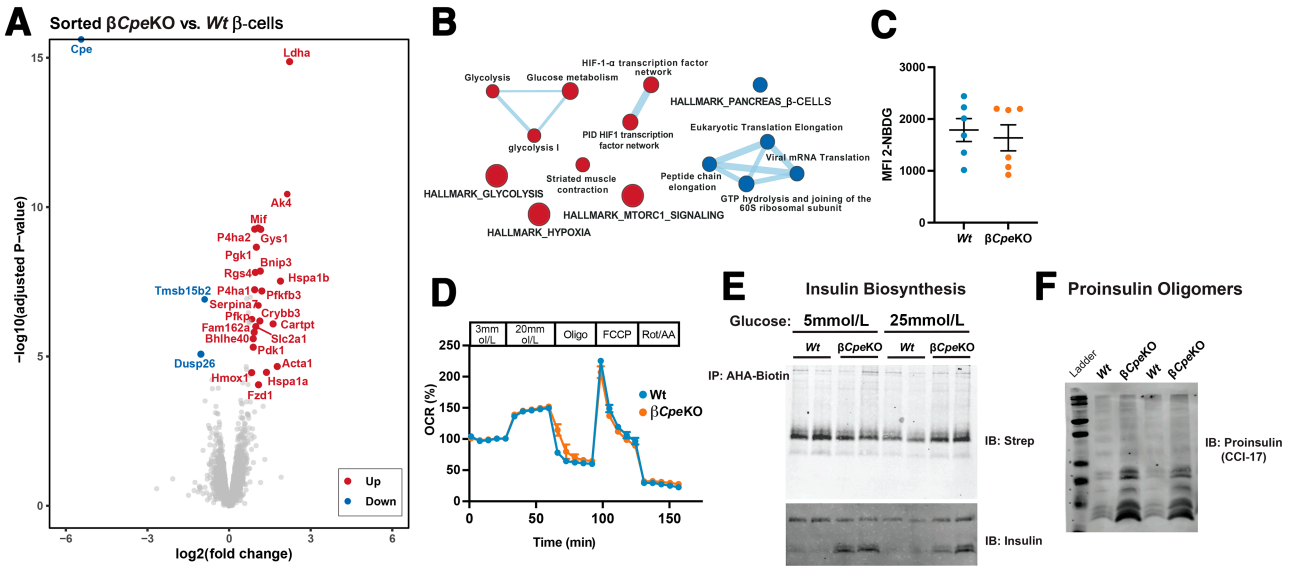

Figure 6—Altered glycolytic transcripts and increased proinsulin biosynthesis in β*Cpe*KO islets. *A*: Transcriptomic analysis of islet β-cells from 16-week-old chow-fed β*Cpe*KO and *Wt* mice ($n = 3$ and 3). Data are presented as a volcano plot with significantly up- or downregulated genes annotated. *B*: Results from GSEA are presented as EnrichmentMap. Red, upregulated gene sets; blue, downregulated gene sets. *C*: Glucose uptake was analyzed by quantifying 2-NBDG fluorescence intensity of dispersed live islet cells from β*Cpe*KO and *Wt* mice via flow cytometer ($n = 6$ and 6). *D*: Baseline-normalized oxygen consumption rate of dispersed islet cells from β*Cpe*KO and *Wt* mice was analyzed (technical triplicate per sample, three samples per genotype). *E*: Freshly isolated islets were equilibrated in methionine-free media and pulsed with 5 mmol/L or 25 mmol/L L-azidohomoalaine (AHA)-containing media for 90 min. Islet protein pellets were click conjugated with biotin alkyne, immunoprecipitated (IP) with avidin, and analyzed with immunoblotting (IB) with use of streptavidin (Strep) and an anti-insulin antibody. *F*: Proinsulin oligomers were analyzed with immunoblotting with an antibody against proinsulin oligomers (monoclonal antibody CCI-17). Down, downregulated; FCCP, carbonyl cyanide 4-(trifluoromethoxy)phenylhydrazone; MFI, mean fluorescence intensity; Oligo, oligomycin; Rot/AA, rotenone and antimycin A; Up, upregulated.

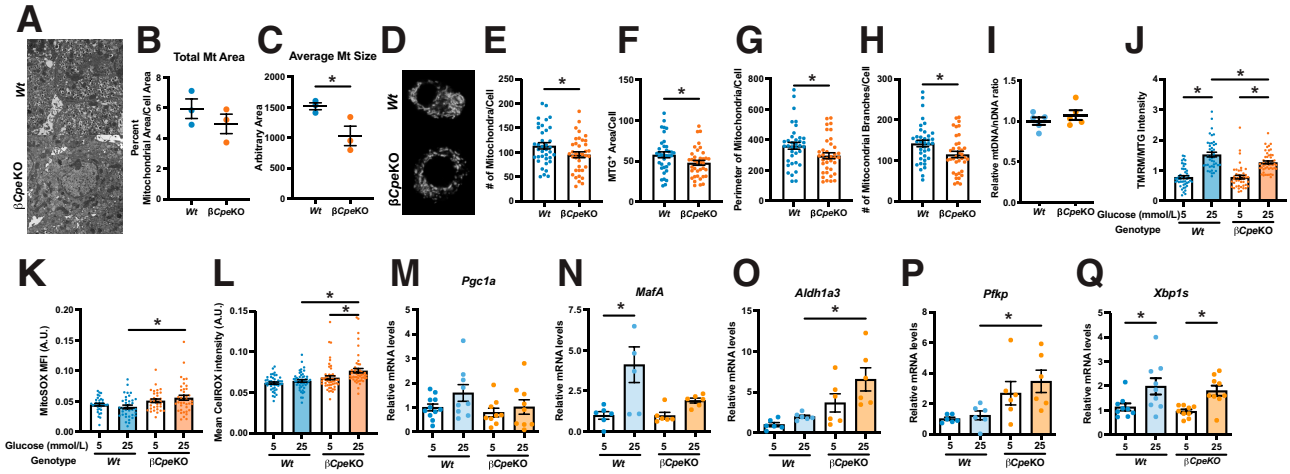

Figure 7—Mitochondrial morphology and function were disturbed in islet cells from β*Cpe*KO mice. *A*: Representative electron micrographs of mitochondria in β-cells from β*Cpe*KO and *Wt* mice. *B* and *C*: Total mitochondria (Mt) area and average mitochondrial size in β-cells were quantified. Each dot represents the average of two to six images from one mouse (>400 mitochondria were analyzed per mouse) (n = 3 per genotype). *D*: Representative immunofluorescence staining of mitochondria with MTG in islet cells from β*Cpe*KO and *Wt* mice. *E–H*: Mitochondria numbers, area, perimeter, and branch number were quantified. Each dot represents one cell, 10–15 cells per mouse, $n \geq 3$ per genotype. *I*: mtDNA content of islets from β*Cpe*KO and *Wt* mice was analyzed with quantitative RT-PCR with ND1 (mtDNA) and 16S (nuclear DNA [nDNA]) primer probes, presented as mtDNA-to-nDNA ratio (n = 5 per genotype). *J–L*: Mitochondrial membrane potential, mitochondrial ROS levels, and cellular ROS levels were analyzed via live cell imaging in 5 mmol/L or 25 mmol/L glucose–treated dispersed islet cells with use of TMRM, MTG, MitoSOX, and CellROX dyes. Each dot represents one cell, 10–15 cells per mouse, $n \geq 3$ per genotype. *M–Q*: Quantitative RT-PCR analysis of *Pgc1α*, *MafA*, *Aldh1a3*, *Pfkp*, *and Xbp1s* in β*Cpe*KO and *Wt* mouse islets treated with 5 mmol/L or 25 mmol/L glucose for 48 h (n = 6 per group). A.U., arbitrary units; MFI, mean fluorescence intensity.

compensating. In agreement with an in vitro study suggesting that Cpe is essential for PC2-mediated peptide processing (25), we showed that loss of Cpe results in reduced PC2 enzyme activity and increased N-terminally extended proIAPP (which is normally processed by PC2 into mature IAPP [23]). Although total islet PC1/3 enzyme activity was not changed in β*Cpe*KO mice, PC1/3 protein levels were elevated, suggesting that on a per-enzyme basis, PC1/3 activity is likely reduced in β*Cpe*KO β-cells. To our surprise, even with markedly impaired proinsulin processing and diminished output of mature insulin, β*Cpe*KO mice failed to develop obesity and hyperglycemia

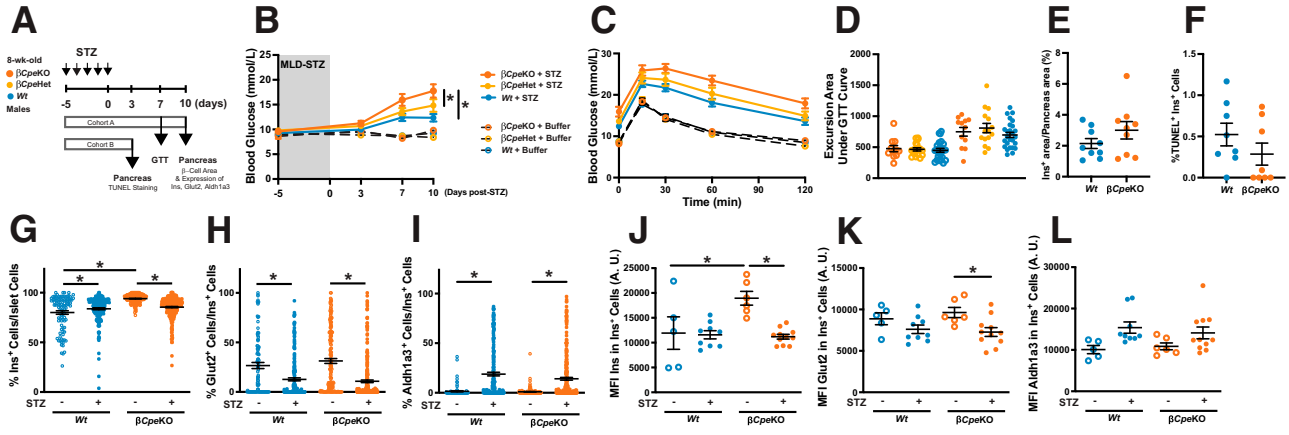

Figure 8—β*Cpe*KO mice have accelerated development of MLD-STZ–induced hyperglycemia. *A*: Timeline of MLD-STZ experiment. *B*: Fasting blood glucose levels of β*Cpe*KO and littermate mice administered with a buffer (empty circle with dotted line) or MLD-STZ (filled circle with solid line). *C* and *D*: IPGTT was performed 7 days after the last STZ injection, and excursion area under the glucose tolerance test curve was analyzed ($n \geq 10$ per group). *E*: β-Cell area of MLD-STZ–treated β*Cpe*KO and *Wt* mice (n = 9 and 9). *F*: β-Cell death was analyzed with use of pancreatic sections of MLD-STZ–treated β*Cpe*KO and *Wt* mice with TUNEL and insulin staining (n = 8 and 8). *G–L*: Frequency and staining intensity of insulin$^+$, Glut2$^+$, and Aldh1a3$^+$ cells in pancreatic sections of MLD-STZ β*Cpe*KO and *Wt* mice were analyzed. (*G–I*: Each dot represents one islet. *J–L*: Each dot represents average fluorescent intensity of islets from one pancreatic section of one mouse; $n \geq 5$ per group.) AUC, area under the curve; A.U., arbitrary units; GTT, glucose tolerance test; MFI, mean fluorescence intensity.

spontaneously or when challenged with an HFD, contrary to a recent report that *Pdx-Cre*^{ERT}-mediated *Pcsk1* deletion and elevated proinsulin promote the development of obesity in mice (33). It is plausible that elevated proinsulin, possessing 5% activity compared with insulin (34,35), is sufficient to maintain glucose homeostasis. Another possibility is that obesity and overt hyperglycemia observed in *Cpe* mutations are driven by insufficient *Cpe* and defective neuropeptide processing in other tissues, such as in the hypothalamus, although mice with *Cpe* deletion in proopiomelanocortin (POMC)-expressing neurons do not become obese (36). Whether Cpe controls body weight and metabolic homeostasis in non-POMC-expressing neuroendocrine cells remains to be tested.

β-Cells are able to adapt to increased insulin demand by increasing production, secretion, and mass prior to hyperglycemia onset (37–39). β*Cpe*KO mice have increased proinsulin production and elevated β-cell area but remain normoglycemic. Because protein overproduction may change intrinsic metabolic pathways and alter β-cell fate (40), it is plausible that increased demand caused by increased insulin production (41) contributes to metabolic pathway rewiring and concomitant β-cell proliferation in β*Cpe*KO mice. In a recent large-scale small molecule screen a compound was identified that promotes protein synthesis and β-cell regeneration. The authors showed that the increased β-cell regeneration is associated with hypo-translation of mRNAs that are integral to mitochondrial-related processes (42). In support of this idea, we observed altered glycolytic gene signatures and changes in mitochondrial morphology and membrane potential in β*Cpe*KO β-cells. Oxygen consumption rate was not reduced in islets from β*Cpe*KO mice, hinting that additional pathological stimuli are likely needed to disrupt oxidative phosphorylation. Alternatively, metabolic flux analysis may offer more quantitative insights into carbon metabolism and energy flow in islets with inherently elevated proinsulin biosynthesis. It is also possible that the increased proinsulin oxidative folding burden may create ER redox imbalances (43), leading to increased mitochondrial and cellular ROS levels. Future live-cell imaging experiments with ROS biosensors could illuminate the cellular sequence of events. Both mild ER stress and ROS have been reported to facilitate β-cell proliferation (16,44). Despite an accumulation of proinsulin oligomers (28), we failed to detect significant changes in transcripts encoding ER chaperons or unfolded protein response proteins. Of note, β-cell dedifferentiation markers *Serpina7* (45) and *Ldha* (46) are reduced in sorted β-cells from normoglycemic β*Cpe*KO mice, suggesting that the slight loss of β-cell identity may occur during early-stage β-cell compensation prior to the development of hyperglycemia. Whether insulin biosynthesis impacts insulin granule secretion requires further investigation. We speculated that increased proinsulin biosynthesis burden and altered glucose metabolism or redox handling capacity may contribute to defects in coupling or translocation of granules to the site of Ca^{2+} channels, which results in reduced exocytotic response of β*Cpe*KO β-cells to a train of membrane depolarizations. Alternatively, increased insulin production may affect the composition of the secretory granule membrane (47), which alters its interaction with plasma membrane Ca^{2+} channels or the fusion with plasma membrane (48). It is also worth mentioning that we have not analyzed possible changes in paracrine signaling in β*Cpe*KO islets.

β*Cpe*KO mice adapted to chronic dietary stress weight gain and glucose tolerance similar to those of their littermates. We administered β*Cpe*KO mice and their littermates with MLD-STZ to induce acute insulin secretory stress without extensive β-cell death or loss of β-cell mass. MLD-STZ led to loss of β-cell identity in both *Wt* and β*Cpe*KO mice, evidenced by an increased percentage of *Aldh1a3*$^{+}$ cells and reduced Glut2^{+} cells in islets. After MLD-STZ, β*Cpe*KO mice also had accelerated development of hyperglycemia and displayed reduced (pro)insulin and Glut2 expression levels in β-cells. These findings were mirrored in vitro, as we observed no induction of *MafA*, and increased *Aldh1a3,* in high glucose–treated β*Cpe*KO islets. We speculate that suboptimal mitochondrial function, or altered cellular redox homeostasis, resulting from the combination of secretory stress and *Cpe* deficiency, contributes to β-cell dysfunction in MLD-STZ *Cpe*-deficient islets (49–51). It has been reported that islets from *Cpe* mutant mice are more susceptible to palmitic acid–induced β-cell apoptosis (32). We were unable to observe detectable differences in TUNEL^{+} β-cells in MLD-STZ–treated β*Cpe*KO 3 days after the last STZ injection, when β-cell apoptosis rates are at their highest (52). Instead, β-cells from β*Cpe*KO mice have reduced Glut2 expression, which may present an adaptive mechanism to attenuate glucose uptake and metabolic stress–induced β-cell death (53).

In summary, we demonstrated that loss of *Cpe* in pancreatic β-cells does not contribute to spontaneous development of obesity and hyperglycemia in mice. However, elevated proinsulin output likely reshapes β-cell glucose metabolism and increases its susceptibility to secretory stress–induced dysfunction and diabetes. Our model may shed light on β-cell translational adaptation, which likely occurs early during the development of diabetes. Additional studies in other prediabetes models and human islets are needed for a better understanding of these early adaptive events and will aid discovery of new therapeutic targets to preserve β-cell function prior to the onset of diabetes.

Acknowledgments. The authors thank Dr. Paul Orban (University of British Columbia) for helpful comments on the project, Dr. Iris Lindberg (University of Maryland Medical Center) for providing the enzyme activity assay protocol and reagents, Dr. Rohit Sharma (University of Massachusetts Amherst) and Dr. Aaron Cox (Baylor College of Medicine) for providing suggestions on β-cell proliferation experiments, Mr. Daniel Pausula (University of British Columbia) for providing protocol for live cell imaging experiments, Drs. Lei Dei and Galina Soukhatcheva (University of British Columbia) for technical

assistance, and Dr. Elizabeth Simpson (University of British Columbia) for help with mouse rederivation.

Funding. This work is supported by JDRF (advanced postdoctoral fellowship 3-APF-2022-1141-A-N to Y.-C.C.), Canadian Institutes of Health Research (grant PJT-153156 to C.B.V.), BC Children's Hospital Foundation and BC Children's Hospital Research Institute (Canucks for Kids Fund Childhood Diabetes Laboratories Summer Studentship to K.L.C.W.), Natural Sciences and Engineering Research Council of Canada (NSERC) grant RGPIN-2020-05390946 and Michael Smith Health Research BC Scholar Award to R.I.K.-G., and National Institutes of Health grants R01DK122160 and U01DK124020 to W.-J.Q. Mass spectrometry proteomics experiments were performed in the Environmental Molecular Sciences Laboratory, Pacific Northwest National Laboratory, a national scientific user facility sponsored by the Department of Energy under contract DE-AC05-76RL0 1830.

Duality of Interest. No potential conflicts of interest relevant to this article were reported.

Author Contributions. Y.-C.C. contributed to study conceptualization, investigation, formal analysis, and visualization and wrote the manuscript. A.J.T. contributed to study conceptualization and investigation and edited the manuscript. J.M.F., X.-Q.D., and M.K. contributed to study methodology, investigation, and formal analysis. K.L.C.W. contributed to study investigation and formal analysis and edited the manuscript. K.F. and A.E.P. contributed to study investigation. A.C.S. contributed to study investigation and methodology and edited the manuscript. R.I.K.-G. contributed to study methodology and formal analysis. P.E.M. and W.-J.Q. contributed to study investigation and methodology. C.B.V. contributed to study conceptualization and investigation and reviewed and edited the manuscript. All authors approved the final version of the manuscript. C.B.V. is the guarantor of this work and, as such, had full access to all the data in the study and takes responsibility for the integrity of the data and the accuracy of the data analysis.

Prior Presentation. Parts of this study were presented in abstract form at the 55th Annual Meeting of the European Association for the Study of Diabetes, Barcelona, Spain, 16–20 September 2019; the 58th Annual Meeting of the European Association for the Study of Diabetes, 19–23 September 2022, Stockholm, Sweden; and the Gordon Research Conference on Protein Processing, Trafficking and Secretion, New London, NH, 17–22 July 2022.

References

1. Zhu X, Orci L, Carroll R, Norrbom C, Ravazzola M, Steiner DF. Severe block in processing of proinsulin to insulin accompanied by elevation of des-64,65 proinsulin intermediates in islets of mice lacking prohormone convertase 1/3. Proc Natl Acad Sci U S A 2002;99:10299–10304

2. Furuta M, Carroll R, Martin S, et al. Incomplete processing of proinsulin to insulin accompanied by elevation of Des-31,32 proinsulin intermediates in islets of mice lacking active PC2. J Biol Chem 1998;273:3431–3437

3. Davidson HW, Hutton JC. The insulin-secretory-granule carboxypeptidase H. Purification and demonstration of involvement in proinsulin processing. Biochem J 1987;245:575–582

4. Wei FY, Suzuki T, Watanabe S, et al. Deficit of tRNA(Lys) modification by Cdkal1 causes the development of type 2 diabetes in mice. J Clin Invest 2011;121:3598–3608

5. Tran DT, Pottekat A, Mir SA, et al. Unbiased profiling of the human proinsulin biosynthetic interaction network reveals a role for peroxiredoxin 4 in proinsulin folding. Diabetes 2020;69:1723–1734

6. Liu M, Huang Y, Xu X, et al. Normal and defective pathways in biogenesis and maintenance of the insulin storage pool. J Clin Invest 2021;131:142240

7. Lu H, Yang Y, Allister EM, Wijesekara N, Wheeler MB. The identification of potential factors associated with the development of type 2 diabetes: a quantitative proteomics approach. Mol Cell Proteomics 2008;7:1434–1451

8. Kahn SE, Chen YC, Esser N, et al. The β cell in diabetes: integrating biomarkers with functional measures. Endocr Rev 2021;42:528–583

9. Alsters SIM, Goldstone AP, Buxton JL, et al. Truncating homozygous mutation of carboxypeptidase E (CPE) in a morbidly obese female with type 2 diabetes mellitus, intellectual disability and hypogonadotrophic hypogonadism. PLoS One 2015;10:e0131417

10. Chen H, Jawahar S, Qian Y, et al. Missense polymorphism in the human carboxypeptidase E gene alters enzymatic activity. Hum Mutat 2001;18:120–131

11. Durmaz A, Aykut A, Atik T, et al. A new cause of obesity syndrome associated with a mutation in the carboxypeptidase gene detected in three siblings with obesity, intellectual disability and hypogonadotropic hypogonadism. J Clin Res Pediatr Endocrinol 2021;13:52–60

12. Cawley NX, Zhou J, Hill JM, et al. The carboxypeptidase E knockout mouse exhibits endocrinological and behavioral deficits. Endocrinology 2004;145:5807–5819

13. Naggert JK, Fricker LD, Varlamov O, et al. Hyperproinsulinaemia in obese fat/fat mice associated with a carboxypeptidase E mutation which reduces enzyme activity. Nat Genet 1995;10:135–142

14. Chen YC, Mains RE, Eipper BA, et al. PAM haploinsufficiency does not accelerate the development of diet- and human IAPP-induced diabetes in mice. Diabetologia 2020;63:561–576

15. Mosser RE, Maulis MF, Moullé VS, et al. High-fat diet-induced β-cell proliferation occurs prior to insulin resistance in C57Bl/6J male mice. Am J Physiol Endocrinol Metab 2015;308:E573–E582

16. Sharma RB, O'Donnell AC, Stamateris RE, et al. Insulin demand regulates β cell number via the unfolded protein response. J Clin Invest 2015;125:3831–3846

17. Blanco EH, Ramos-Molina B, Lindberg I. Revisiting PC1/3 mutants: dominant-negative effect of endoplasmic reticulum-retained mutants. Endocrinology 2015;156:3625–3637

18. Dai XQ, Plummer G, Casimir M, et al. SUMOylation regulates insulin exocytosis downstream of secretory granule docking in rodents and humans. Diabetes 2011;60:838–847

19. Fulcher JM, Makaju A, Moore RJ, et al. Enhancing top-down proteomics of brain tissue with FAIMS. J Proteome Res 2021;20:2780–2795

20. Liu M, Ramos-Castañeda J, Arvan P. Role of the connecting peptide in insulin biosynthesis. J Biol Chem 2003;278:14798–14805

21. Chaudhry A, Shi R, Luciani DS. A pipeline for multidimensional confocal analysis of mitochondrial morphology, function, and dynamics in pancreatic β-cells. Am J Physiol Endocrinol Metab 2020;318:E87–E101

22. Marzban L, Trigo-Gonzalez G, Zhu X, et al. Role of beta-cell prohormone convertase (PC)1/3 in processing of pro-islet amyloid polypeptide. Diabetes 2004;53:141–148

23. Wang J, Xu J, Finnerty J, Furuta M, Steiner DF, Verchere CB. The prohormone convertase enzyme 2 (PC2) is essential for processing pro-islet amyloid polypeptide at the NH2-terminal cleavage site. Diabetes 2001;50:534–539

24. Marzban L, Soukhatcheva G, Verchere CB. Role of carboxypeptidase E in processing of pro-islet amyloid polypeptide in beta-cells. Endocrinology 2005;146:1808–1817

25. Zhu X, Rouille Y, Lamango NS, Steiner DF, Lindberg I. Internal cleavage of the inhibitory 7B2 carboxyl-terminal peptide by PC2: a potential mechanism for its inactivation. Proc Natl Acad Sci U S A 1996;93:4919–4924

26. Chu KY, Briggs MJL, Albrecht T, Drain PF, Johnson JD. Differential regulation and localization of carboxypeptidase D and carboxypeptidase E in human and mouse β-cells. Islets 2011;3:155–165

27. Cattin-Ortolá J, Topalidou I, Lau H-T, et al. CCDC186 controls dense-core vesicle cargo sorting by exit. 6 November 2019 [preprint]. bioRxiv:616458

28. Arunagiri A, Haataja L, Pottekat A, et al. Proinsulin misfolding is an early event in the progression to type 2 diabetes. eLife 2019;8:e44532

29. Liew CW, Assmann A, Templin AT, et al. Insulin regulates carboxypeptidase E by modulating translation initiation scaffolding protein eIF4G1 in pancreatic β cells. Proc Natl Acad Sci U S A 2014;111:E2319–E2328

30. Blandino-Rosano M, Barbaresso R, Jimenez-Palomares M, et al. Loss of mTORC1 signalling impairs β-cell homeostasis and insulin processing. Nat Commun 2017;8:16014

31. Lee AH, Heidtman K, Hotamisligil GS, Glimcher LH. Dual and opposing roles of the unfolded protein response regulated by IRE1α and XBP1 in proinsulin processing and insulin secretion. Proc Natl Acad Sci U S A 2011; 108:8885–8890
32. Jeffrey KD, Alejandro EU, Luciani DS, et al. Carboxypeptidase E mediates palmitate-induced β-cell ER stress and apoptosis. Proc Natl Acad Sci U S A 2008;105:8452–8457
33. Meier DT, Rachid L, Wiedemann SJ, et al. Prohormone convertase 1/3 deficiency causes obesity due to impaired proinsulin processing. Nat Commun 2022;13:4761
34. Bergenstal RM, Cohen RM, Lever E, et al. The metabolic effects of biosynthetic human proinsulin in individuals with type I diabetes. J Clin Endocrinol Metab 1984;58:973–979
35. Yu SS, Kitbachi AE. Biological activity of proinsulin and related polypeptides in the fat tissue. J Biol Chem 1973;248:3753–3761
36. Fricker LD, Tashima AK, Fakira AK, Hochgeschwender U, Wetsel WC, Devi LA. Neuropeptidomic analysis of a genetically defined cell type in mouse brain and pituitary. Cell Chem Biol 2021;28:105–112.e4
37. Boland BB, Rhodes CJ, Grimsby JS. The dynamic plasticity of insulin production in β-cells. Mol Metab 2017;6:958–973
38. Kahn SE, Prigeon RL, McCulloch DK, et al. Quantification of the relationship between insulin sensitivity and β-cell function in human subjects: evidence for a hyperbolic function. Diabetes 1993;42:1663–1672
39. Weir GC, Bonner-Weir S. Five stages of evolving beta-cell dysfunction during progression to diabetes. Diabetes 2004;53(Suppl. 3):S16–S21
40. Montemurro C, Nomoto H, Pei L, et al. Publisher correction: IAPP toxicity activates HIF1α/PFKFB3 signaling delaying β-cell loss at the expense of β-cell function. Nat Commun 2019;10:3507
41. Rumala CZ, Liu J, Locasale JW, Corkey BE, Deeney JT, Rameh LE. Exposure of pancreatic β-cells to excess glucose results in bimodal activation of mTORC1 and mTOR-dependent metabolic acceleration. iScience 2020; 23:100858
42. Karampelias C, Watt K, Mattsson CL, et al. MNK2 deficiency potentiates β-cell regeneration via translational regulation. Nat Chem Biol 2022;18:942–953
43. Elksnis A, Martinell M, Eriksson O, Espes D. Heterogeneity of metabolic defects in type 2 diabetes and its relation to reactive oxygen species and alterations in beta-cell mass. Front Physiol 2019;10:107
44. Ahmed Alfar E, Kirova D, Konantz J, Birke S, Mansfeld J, Ninov N. Distinct levels of reactive oxygen species coordinate metabolic activity with beta-cell mass plasticity. Sci Rep 2017;7:3994
45. Kim-Muller JY, Fan J, Kim YJR, et al. Aldehyde dehydrogenase 1a3 defines a subset of failing pancreatic β cells in diabetic mice. Nat Commun 2016;7:12631
46. Sekine N, Cirulli V, Regazzi R, et al. Low lactate dehydrogenase and high mitochondrial glycerol phosphate dehydrogenase in pancreatic beta-cells. Potential role in nutrient sensing. J Biol Chem 1994;269:4895–4902
47. MacDonald MJ, Ade L, Ntambi JM, Ansari IUH, Stoker SW. Characterization of phospholipids in insulin secretory granules and mitochondria in pancreatic beta cells and their changes with glucose stimulation. J Biol Chem 2015;290:11075–11092
48. Kreutzberger AJB, Kiessling V, Doyle CA, et al. Distinct insulin granule subpopulations implicated in the secretory pathology of diabetes types 1 and 2. Elife 2020;9:e62506
49. Guo S, Dai C, Guo M, et al. Inactivation of specific β cell transcription factors in type 2 diabetes. J Clin Invest 2013;123:3305–3316
50. Maechler P, Jornot L, Wollheim CB. Hydrogen peroxide alters mitochondrial activation and insulin secretion in pancreatic beta cells. J Biol Chem 1999;274: 27905–27913
51. Leenders F, Groen N, de Graaf N, et al. Oxidative stress leads to β-cell dysfunction through loss of β-cell identity. Front Immunol 2021;12:690379
52. O'Brien BA, Harmon BV, Cameron DP, Allan DJ. Beta-cell apoptosis is responsible for the development of IDDM in the multiple low-dose streptozotocin model. J Pathol 1996;178:176–181
53. Gottmann P, Speckmann T, Stadion M, et al. Heterogeneous development of β-cell populations in diabetes-resistant and -susceptible mice. Diabetes 2022;71:1962–1978